Metastable-defect behavior in silicon: Charge-state-controlled reorientation of iron-aluminum pairs

Alain Chantre and Daniel Bois
Centre National d'Etudes des Télécommunications, Chemin du Vieux Chêne, Boite Postale 98, F-38243 Meylan Cedex, France
(Received 26 December 1984)

We report the observation of a novel example of defect metastability in silicon. The phenomenon, monitored by deep-level transient spectroscopy, takes place at a well-identified point defect, i.e., the interstitial-iron—substitutional-aluminum pair ($Fe_{(i)}Al_{(s)}$). The charge state of the defect during sample cooldown to low temperature is found to control a reversible transmutation behavior between two defect energy levels, at $E_V+0.20$ eV (H1) and $E_V+0.13$ eV (H2). A kinetic study of the transformation has led to a detailed microscopic description of the phenomenon. It is shown to arise from a charge-state-controlled, electrostatically driven, reorientation of $Fe_{(i)}Al_{(s)}$ pairs between ⟨111⟩ and ⟨100⟩ configurations. Levels H1 and H2 are thus ascribed to $(Fe_{(i)})^{2+}$-$(Fe_{(i)})^{+}$ transitions at the nearest and next-nearest tetrahedral sites adjacent to aluminum, respectively. A configuration-coordinate (CC) description of the center, based on the simple ionic model of iron-acceptor pairs, is shown to account for all features of the reaction. No very large lattice relaxation is needed to understand the phenomenon. The CC model of the $Fe_{(i)}Al_{(s)}$ pair is then extended to non-purely-ionic defect complexes. A complete new class of metastable centers is thus proposed. Metastable phenomena involving other semiconductor defects (*A* center in silicon, EL2 center in GaAs, *M* center in InP) are discussed in the light of these new CC models.

I. INTRODUCTION: IRON-ACCEPTOR PAIRS IN SILICON

Iron is the most intensively investigated $3d$ transition-metal impurity in silicon.[1] Because of its high solubility and fast diffusivity at high temperature, it is easily introduced into silicon crystals during heat treatments. Usually present in the electrically inactive precipitated form, iron atoms become active when individually dispersed into the crystal upon thermal processes such as fast cooling or quenching.[2,3] Iron then forms a deep donor center at $E_V+0.38$ eV (Ref. 4) detectable by electron paramagnetic resonance (EPR) as iron on a tetrahedral (T_d) interstitial site.[5] Because of its low migration energy, $E_m=0.68$ eV,[1] interstitial iron ($Fe_{(i)}$) is mobile even down to room temperature. In *p*-type material, mobile positively charged iron ions $Fe_{(i)}^{+}$ are captured by negative (substitutional) shallow acceptors $A_{(s)}^{-}$, with the formation of iron-acceptor pairs, $Fe_{(i)}A_{(s)}$.[5]

The microscopic structure of transition-metal—acceptor pairs has been known since the early EPR work of Ludwig and Woodbury.[5] With the exception of $Fe_{(i)}In_{(s)}$, which shows ⟨100⟩ symmetry, all such pairs have ⟨111⟩ axial symmetry, consistent with the simplest pair model of a substitutional negatively charged acceptor impurity with a positively charged transition metal on the nearest interstitial site. The resonance properties of the pairs are in accord with the ionic model. Iron-acceptor pairs are also electrically active, and have been identified by deep-level transient spectroscopy (DLTS).[4,6] They form donor levels in the lower half of the band gap, associated with $(Fe_{(i)})^{+}(A_{(s)})^{-}$-$(Fe_{(i)})^{2+}(A_{(s)})^{-}$ transitions. Pair formation and dissociation around room temperature have been extensively studied using DLTS.[6–8] The results are properly described within the framework developed by Reiss *et al.*[9] for ion pairing.[10] The pair binding energy is close to 0.5 eV, in accordance with the model of two electrostatistically bound point charges[7,8] [$E_b=e^2/\epsilon r_1=0.52$ eV, where ϵ is the dielectric constant of silicon, r_1 the distance between the nearest T_d interstitial site and the substitutional site (2.35 Å), and e the electron charge].

Within the framework of this simple ionic model, one would expect to observe other configurations of the pairs, at least the ⟨100⟩ configuration with $Fe_{(i)}$ sitting in the next-nearest T_d interstitial site adjacent to $A_{(s)}$ ($r_2=2.72$ Å). The additional energy required to produce a first- to second-nearest-neighbor separation is indeed fairly low:

$$\Delta E_b=\frac{e^2}{\epsilon}\left[\frac{1}{r_1}-\frac{1}{r_2}\right]\sim 0.071 \text{ eV} , \tag{1}$$

for iron in the $Fe_{(i)}^{+}$ charge state. Therefore, the fraction of $(Fe_{(i)})^{+}(A_{(s)}^{-})$ pairs aligned along a ⟨100⟩ direction, calculated as

$$f\sim\exp[-(0.071 \text{ eV})/kT] , \tag{2}$$

should be significant.

Moreover, one would predict the observation of an additional energy level in the band gap for those pairs oriented along the ⟨100⟩ direction. This is best demonstrated by the configuration-coordinate (CC) diagram shown in Fig. 1, constructed from simple electrostatic arguments. Because of the higher-, i.e., double-, energy difference between the two pair configurations for iron in the $Fe_{(i)}^{2+}$ charge state, $(Fe_{(i)})^{+}$-$(Fe_{(i)})^{2+}$ transitions at

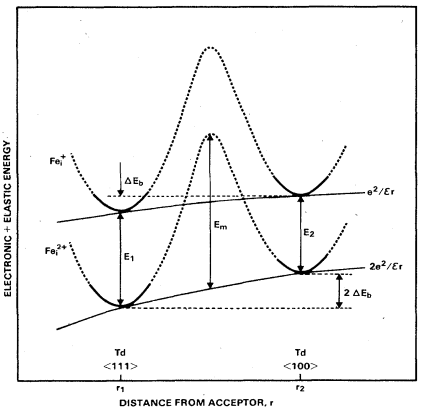

FIG. 1. Configuration-coordinate diagram for iron-acceptor pairs in silicon. The model is based on a Coulomb interaction potential between the two impurities. E_m is the barrier to atomic motion of iron from one configuration to the other.

the second T_d site would be expected at energy

$$E_2 = E_1 - \Delta E_b = E_1 - 0.071 \text{ eV} , \quad (3)$$

compared to energy E_1 for the nearest site. The simple ionic model illustrated in Fig. 1 also reveals that the fraction of pairs in the $\langle 100 \rangle$ configuration detected at low temperature, e.g., as in a DLTS experiment, would depend on the defect charge state during the cooldown procedure: It would be much higher for the defect prepared in the neutral $[(Fe_{(i)})^+(Al_{(s)})^-]$ state. In other words, one would expect irreproducible spectral changes to be observed for such iron-acceptor pairs, without perfect control of the electronic, thermal, and optical history of the system.

Examples of such defect metastability have already been reported in silicon and indium phosphide following MeV electron irradiation.[11] No microscopic explanation of these effects has been given so far, although configuration-coordinate descriptions of the phenomena, based on large lattice relaxations, have been proposed.[12] We have recently discovered a new case of metastable-defect behavior in silicon, which takes place at the interstitial-iron—substitutional-aluminum pair, $Fe_{(i)}Al_{(s)}$.[13] This paper describes the results of a comprehensive study of the phenomenon. All the features of the simple ionic model discussed above appear to be fully confirmed. We are thus led to a more complete understanding of the configurational instability than for any other metastable center in covalent semiconductors. It is ascribed to charge-state-controlled, electrostatically driven single-jump motion of $Fe_{(i)}$ in the vicinity of $Al_{(s)}$. Extension of the model to non-purely-ionic defect complexes is then shown to provide clues for the understanding of other metastable-defect phenomena in semiconductors.

The paper is organized as follows. In Sec. II we detail our capacitance spectroscopic data on the $Fe_{(i)}Al_{(s)}$ pair in silicon and its configurational instability. A CC model of the center is then constructed from these data, which confirms the Coulombic nature of the interaction potential. In Sec. III we extend the double-site CC-diagram concept to non-purely-ionic centers. Metastable phenomena involving other semiconductor defects (A center in Si, EL2 center in GaAs, M center in InP) are then discussed in the light of these new CC models. Section IV contains our concluding remarks.

II. RESULTS: IRON-ALUMINUM PAIR IN SILICON

A. Experimental details

The material used in this work consisted of p-type aluminum-doped silicon substrates ($p \sim 10^{16}$ cm^{-3}). Both float-zone-refined and Czochralski-grown crystals were used, without any difference in the results to be described. No defect levels were found at concentrations higher than $\sim 10^{12}$ cm^{-3} in the samples during preliminary DLTS characterization.

Iron-aluminum pairs were produced by sweeping the focused beam of a cw argon laser across the front surface of bare wafers. Previous studies[3,14,15] have shown that iron-acceptor pairs are the dominant defects resulting from such ultrashort heat treatments. Details on the process and the heat treatments induced in the samples may be found elsewhere.[16,17]

The metastable-defect phenomenon was studied using DLTS. The main features of our experimental setup include fast-capacitance transient detection (time constant ~ 3 μsec), lock-in-amplifier rate-window setting, and computer control of the system.[16] All measurements were performed in darkness using Schottky-barrier structures fabricated by evaporation of aluminum through a metal mask.

The basic procedure used to reveal the configurational instability of the $Fe_{(i)}Al_{(s)}$ center is similar to the method described by Benton and Levinson in their report of metastable-defect phenomena in Si and InP.[11] It involves the application or absence of a reverse bias during the cooling of the sample from room temperature to the initial measurement temperature (77 K). In the former case no carriers are present in the active region of the device (the space-charge region of the diode) during sample cooldown; defects are thus prepared in their less positive charge state. The more positive one is selected in the latter case, due to the presence of free holes in the same region of the sample. Afterward, a conventional DLTS spectrum with periodic hole trapping and detrapping is recorded while heating up the sample.

B. Results

A typical DLTS spectrum of the defect states observed in ultrafast-quenched Al-doped silicon is shown in Fig. 2. Two major defects, labeled H1 and H2, are detected, with respective hole-emission activation energies of 0.20 and 0.13 eV.[18] These two levels have been observed previously in Al-doped Si following iron diffusion and quenching.[4,6] H1 was identified as the donor level of the $Fe_{(i)}Al_{(s)}$ pair, whereas no specific assignment was reported for H2.[1,4] The third trap, H3 (hole-emission activation energy 0.52 eV) is unique to ultrafast-quenched (cw-laser-irradiated)

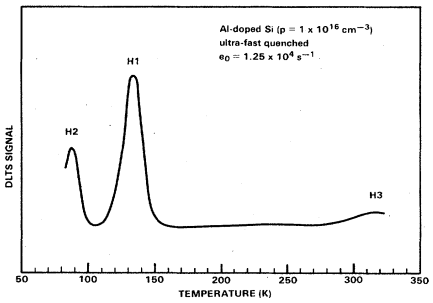

FIG. 2. DLTS spectrum for Al-doped silicon. Ultrafast quenching displays the H1 ($Fe_{(i)}Al_{(s)}$), H2 (hitherto unidentified), and H3 (Al-V) features.

Al-doped material, and has been recently identified as associated with quenched-in aluminum-vacancy pairs.[19]

The configurational instability of the $Fe_{(i)}Al_{(s)}$ pair is demonstrated in Fig. 3, which displays the low-energy part of the observed DLTS spectrum ($T < 150$ K), following (a) sample cooldown under reverse bias or (b) zero-bias conditions. The unexpected observation is the dramatic complementary behavior of the two DLTS peaks: cooling the sample with free holes present (an unusual procedure in DLTS measurements) has almost completely cleared the H2 signal, while peak H1 has grown correspondingly. The phenomenon was found to be completely reversible: Each of the two characteristic spectra could be exactly and instantaneously reproduced, provided that the sample was cooled from above 250 K under the proper bias condition.

The reversible, correlated behavior of the H1 and H2 signal amplitudes strongly suggests that this metastable-defect reaction is associated with an internal rearrangement of a single center, i.e., the $Fe_{(i)}Al_{(s)}$ pair. This statement was confirmed by complementary, spatially resolved DLTS data. Figure 4 shows the depth distribution of defect H1 below the Al/Si interface, as measured following three different cooldown conditions: (1) zero-bias cooling, (2) cooling with moderate ($V_R = +2.5$ V) reverse bias, and

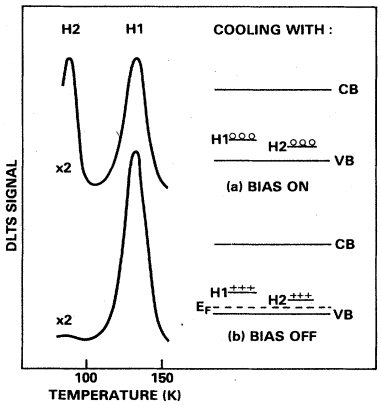

FIG. 3. DLTS spectra of $Fe_{(i)}Al_{(s)}$ in silicon showing the result of cooling with (a) applied reverse bias and (b) zero bias (rate window $e_0 = 1.25 \times 10^4$ s^{-1}).

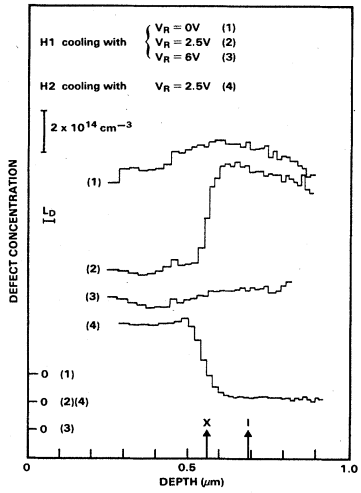

FIG. 4. Spatial depth profiles of the H1 and H2 defect states, following different cooldown conditions. The quoted L_D, X, and l values (see text) correspond to $T = 126$ K (H1 profiles measurement temperature). Note the different origin on the vertical axis for the various profiles.

(3) cooling with large ($V_R = +6$ V) reverse bias. Also given in the figure is the depth profile of defect H2 observed following cooling type (2). The moderate reverse bias was chosen such that the depletion-layer boundary during sample cooldown be located inside the subsequently investigated surface region of the material (~ 1 μm thick). This would enable a straightforward analysis of the extent of the H1↔H2 transformation with respect to the position of this boundary. The data reveal a sharp—a few Debye lengths (L_D) wide—transition in the depth profiles of the two defects [curves (2) and (4)]. The correlated behavior of the two defect states is locally confirmed. Comparison with zero-bias and large reverse-bias coolings shows that no long-range migration effects are involved. All these findings support the previous suggestion of an internal configurational rearrangement of the $Fe_{(i)}Al_{(s)}$ pair.

The moderate reverse-bias-cooling data in Fig. 4 also reveal the charge-state-controlled nature of the configurational transformation, as opposed to a direct result of the junction electric field. This is demonstrated by the position of the sharp transition in the H1 defect depth profile, with respect to the depletion-layer boundary position (depth 1) and the depth X where the defect energy level crosses the Fermi level within the depletion region. Clearly, the change in defect charge state at depth X controls the H1↔H2 transformation, whereas no specific feature is observed at depth 1, where the junction electric field vanishes. This conclusion is supported by preliminary complementary measurements performed using n^+-p junctions, which show that the transformation may be effected at low temperature under forward-bias electron injection, i.e., in the absence of an electric field.

The transitions from one configuration to the other were investigated in more detail by studying the thermally activated transformation kinetics between states (a) and

(b) of the system (Fig. 3). We used the systematic method presented by Benton *et al.*[11,20] in their study of the metastable M center in InP. In order to examine the transition $a \rightarrow b$, the sample was first cooled from above 250 K to a temperature T with applied reverse bias. The diode was then shorted, and after annealing for a time t at this temperature, the sample was fast-cooled to 77 K. Changes in the populations of the two defect configurations were then detected as changes in the H1 and H2 DLTS peak heights. In the same way, the reverse transition, $b \rightarrow a$, was studied using zero-bias cooling and reverse-bias anneals.

Isochronal (5-min) anneals were first performed to reveal the transformation temperatures. The data are presented in Fig. 5 for both reactions $a \rightarrow b$ and $b \rightarrow a$. The results show that both transitions occur in only one stage, but not at the same temperature: reaction $a \rightarrow b$ is observed at a lower temperature (~ 180 K) than reaction $b \rightarrow a$ (~ 210 K). It is seen also that for these two reactions the changes in DLTS peak heights are such that $\Delta(\mathrm{H1}) = -\Delta(\mathrm{H2})$. Finally, it is noted that both H1 and H2 signals are never zero; H1 even remains the dominant DLTS feature over the entire annealing temperature range. All these results are consistent with the previous observations (Figs. 3 and 4).

The reaction kinetics were then explored around the transformation temperatures by a series of isothermal anneals. The annealing reactions were found to be first order, as demonstrated in Fig. 6 for reaction $a \rightarrow b$. Here, the (normalized) H2 DLTS peak height has been plotted as a function of anneal time and temperature, following the annealing procedure described above. The data fit a simple exponential expression of the form

$$S_{\mathrm{H2}}(t) = [S_{\mathrm{H2}}(0) - S_{\mathrm{H2}}(\infty)]\exp(-Rt) + S_{\mathrm{H2}}(\infty) , \quad (4)$$

as expected for first-order kinetics. Arrhenius plots of the two transformation rates R are shown in Fig. 7. The kinetics for the metastable-defect transitions is consistent with the following relations:

$$R_{a \rightarrow b} = 1 \times 10^{11} \exp[-(0.50\ \mathrm{eV})/kT]\ \mathrm{s}^{-1} , \quad (5)$$

$$R_{b \rightarrow a} = 5 \times 10^{12} \exp[-(0.64\ \mathrm{eV})/kT]\ \mathrm{s}^{-1} . \quad (6)$$

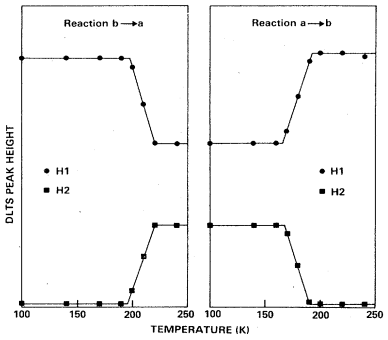

FIG. 5. Isochronal annealing data for the transformations $a \rightarrow b$ and $b \rightarrow a$. For each point, the sample was cooled from 250 K with the appropriate bias condition, annealed for 5 min under the opposite bias condition, and DLTS peaks H1 and H2 were monitored.

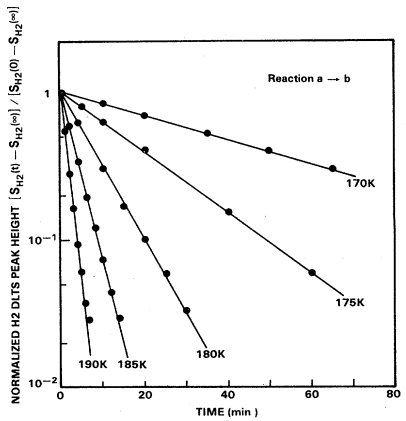

FIG. 6. Isothermal annealing kinetics for reaction $a \rightarrow b$. For each point, the sample was cooled from 250 K to the indicated temperature with applied reverse bias, annealed at zero bias for the indicated time, and DLTS peak H2 was monitored.

In the course of studying the $a \rightarrow b$ transformation kinetics, it was observed that the residual magnitude of the H2 DLTS signal in state (b) was temperature dependent. This is quantitatively shown in Fig. 8, where the asymptotic H2 peak height (normalized to the nearly constant H1 signal) is plotted versus reciprocal temperature. The scatter in the data is rather important. The lower-temperature (~ 181 K) point may be overestimated because of insufficient waiting for thermal equilibrium. Overestimation of the residual signal magnitude is also suspected for the highest temperature (~ 196 K) because of an insufficient fast cool to 77 K.[21] Despite these uncertainties in the measurements, it is apparent that the equilibrium H2 signal amplitude in state (b) is thermally activated, with an activation energy of 0.14 ± 0.01 eV.

Finally, auxiliary experiments were carried out to give additional insight into the electrical and structural properties of the metastable defects and the transformation mechanism. In Fig. 9, a test for acceptor character is applied to the two H1 and H2 defect states by studying the effect of increasing junction electric fields on the carrier-

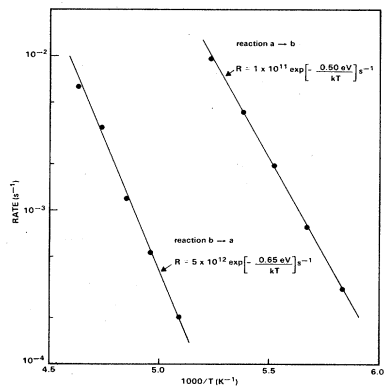

FIG. 7. Reaction kinetics for $a \rightarrow b$ and $b \rightarrow a$ defect transformations.

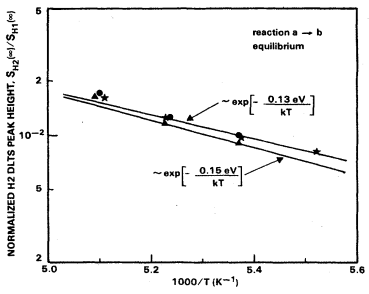

FIG. 8. Thermally activated behavior of the equilibrium H2 DLTS signal amplitude in state (b).

emission processes. Reduction of the filling pulse height from 5 to 0 V at constant reverse voltage (5 V) lowers the average field in the junction from 4.0×10^4 to 5.9×10^3 V/cm. No shift in peak position is detected for H1, confirming its previous assignment to the $Fe_{(i)}Al_{(s)}$ donor level. H2 also does not show the marked motion to higher temperatures—14 K according to the Poole-Frenkel theory[22,23]—expected for hole emission from an acceptor state.[24] We conclude, therefore, that the H2 level is also a donor level, with no long-range Coulombic attraction for a hole. In addition, thermally stimulated capacitance (TSCAP) measurements were performed to reveal any charge change associated with the $b\rightarrow a$ transition. The sample was cooled at zero bias to 50 K, then reverse bias was applied for the TSCAP rewarming procedure. No step in the capacitance-versus-temperature behavior of the junction was detected near 200 K that could be ascribed to the $b\rightarrow a$ transition. Only H1 and H2 responses associated with hole emissions from the space-charge and transition regions of the depletion layer[25] could be observed. These last two experimental data, coupled to the above results, demonstrate that DLTS peaks H1 and H2 arise from two configurations of the $Fe_{(i)}Al_{(s)}$ pairs that correspond to the same charge state.

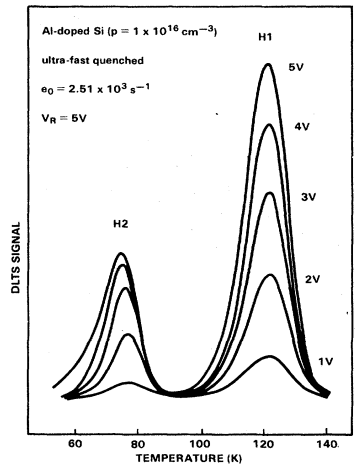

FIG. 9. Electric field effect on hole emission from levels H1 and H2. The absence of a marked shift in peak position reveals the donor character of the centers.

C. Model

All the features of the metastable-defect phenomenon described in Sec. II B may be understood within the framework of the simple ionic model of iron-acceptor pairs illustrated in Fig. 1, with H1 and H2 levels arising from $(Fe_{(i)})^+$-$(Fe_{(i)})^{2+}$ transitions at the nearest and next-nearest T_d sites, respectively. The difference in the activation energies for hole emissions from these two levels ($0.20-0.13=0.07$ eV) is indeed consistent with the value ($\Delta E_b=0.071$ eV) expected for a Coulombic interaction potential (see Sec. I). This level assignment is also in agreement with the charge-state results just presented. The details of the configurational instability are best explained using the CC model of the $Fe_{(i)}Al_{(s)}$ pair shown in Fig. 10, constructed from our experimental data.

When the sample is cooled to 77 K without applied reverse bias, the defect energy levels lie above the Fermi level[26] during the cooling procedure [Fig. 3(b)]. Iron is in the $Fe_{(i)}{}^{2+}$ charge state, and the stable $\langle 111\rangle$ configuration is preferred at the outset of the cooldown (Fig. 10). As a result, the H1 donor level associated with this pair configuration is observed as the major DLTS peak [Fig. 3(b)]. The small H2 signal, arising from the $\langle 100\rangle$ configuration, reflects the fraction of $Fe_{(i)}{}^{2+}$ ions occupying the second-nearest-neighbor position at low temperature. The amplitude of this signal is indeed thermally activated, with the $\sim$0.14 eV energy difference between the two pair configurations. We note that this is the value expected from the simple electrostatic model of Fig. 1 ($2\Delta E_b=0.142$ eV).

When the bias is on during sample cooldown, the quasi-Fermi-level for holes is raised above the defect levels within the extent of the space-charge region, leaving iron in the $Fe_{(i)}{}^+$ charge state. The stable position of the ion is still the nearest T_d site (Fig. 10), but because of a smaller energy difference—$0.14+0.13-0.20=0.07$ eV (against the $\Delta E_b=0.071$ eV expected)—a noticeable fraction of $Fe_{(i)}Al_{(s)}$ pairs occupy the metastable $\langle 100\rangle$ configuration and, hence, we have the spectral changes observed in DLTS [Fig. 3(a)].

The reorientation of $Fe_{(i)}Al_{(s)}$ pairs toward the steady-

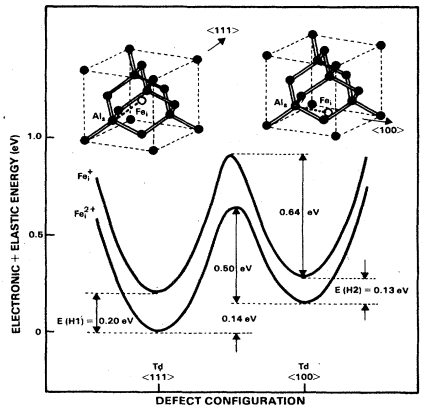

FIG. 10. $Fe_{(i)}Al_{(s)}$ pair in silicon. All the energies quoted on the CC diagram are deduced from the experimental study of the metastable-defect phenomenon.

state occupancy of ⟨111⟩ and ⟨100⟩ configurations gives rise to the experimentally observed $a \rightarrow b$ and $b \rightarrow a$ transitions. The rate of the $a \rightarrow b$ transformation is controlled by the thermally activated jump of $Fe_{(i)}^{2+}$ from the second-nearest to nearest interstitial site (Fig. 10). Similarly, the rate $R(b \rightarrow a)$ originates in the barrier to atomic motion of the $Fe_{(i)}^{+}$ ion from one configuration to the other.[27] Both preexponential factors are indeed in the range expected for a single-jump process (i.e., the lattice-vibration frequency).

The configurational instability displayed by the $Fe_{(i)}Al_{(s)}$ center thus arises from a charge-state-controlled, electrostatically driven partial dissociation of the pair. The metastable ⟨100⟩ pair configuration is detected because of the low migration energy of $Fe_{(i)}$ in silicon, which sets the transformation temperatures to below 300 K. We note that the activation energy for atomic motion of $Fe_{(i)}^{+}$ in the vicinity of $Al_{(s)}^{-}$ (0.64 eV) is in fair agreement with the value (0.65 eV) inferred by Kimerling and Benton[7] near substitutional boron. As suggested by these authors, the difference with the 0.85 eV they measure for the isolated ion in the same temperature range may be ascribed to a residual electrostatic interaction between iron and the acceptor at the saddle point for atomic displacement. The even lower value that we observe for $Fe_{(i)}^{2+}$ near $Al_{(s)}^{-}$ (Fig. 10) is consistent with this suggestion.

D. Discussion

The CC diagram of the $Fe_{(i)}Al_{(s)}$ pair shown in Fig. 10 so closely fits into the simple electrostatic arguments discussed at the beginning that there is little doubt that we are giving the right interpretation for the metastable-defect phenomenon reported in this paper. As a result, we consider as definite the identification of the H2 level as arising from the ⟨100⟩ configuration of the $Fe_{(i)}Al_{(s)}$ pair. This is one of the few—if any—examples in semiconductor defect studies where the microscopic identity of a defect level is established using its sole electronic properties. Confirmation of this has come at the time of writing, from an EPR study of iron-aluminum pairs in silicon by Van Kooten *et al.*[28] These authors report the observation of two spectra, labeled Si-NL27 and Si-NL28, with respective trigonal and rhombic I symmetry, which they identify as ⟨111⟩ and ⟨100⟩-oriented pairs. Experiments are currently being prepared to demonstrate the expected Si-NL27↔Si-NL28 transmutation behavior.

The technique used in this work to obtain structural information on semiconductor defect states should be compared to the stress-induced alignment techniques for point defects in silicon pioneered by Watkins and Corbett.[29] In these experiments, an applied stress is used to remove the orientational degeneracy of a defect which can occupy a set of equivalent sites or orientations, and produce a preferential alignment. The defect alignment is then quenched-in by cooling the sample while maintaining the stress. A symmetry-sensitive technique, such as EPR,[29] polarized excitation optical absorption,[30] or photocapacitance,[31] is finally used to probe this defect alignment. The experiment described in this paper involves a charge-state-controlled preferential alignment of a defect among nonequivalent orientations. The sample is then cooled while controlling the defect charge state, and the alignment is quenched-in. DLTS is subsequently used to probe the defect alignment, through the distinct electronic properties of the various nonequivalent orientations. As for the stress-induced alignment techniques, the defect reorientation lifetime may be measured by studying the recovery kinetics of the charge-state-controlled, characteristic defect-state spectrum.

III. DISCUSSION: METASTABLE CENTERS IN SEMICONDUCTORS

A. Extension of the double-site CC diagram

The CC diagram constructed to explain the spectroscopic data relating to the iron-aluminum pair in silicon and its configurational transformation should be briefly discussed within the general context of lattice-relaxation phenomena. Whereas most recent examples[12,32–34] of metastable-defect behavior in covalent semiconductors have been ascribed to strong electron-lattice interactions and phenomenologically explained using large lattice-relaxation models, the CC diagram presented in this paper to explain the unusual properties of the $Fe_{(i)}Al_{(s)}$ center puts it into the more familiar class of "ordinary" defects.[35] The CC model shown in Fig. 10 is even of the zero-relaxation type, i.e., with no lattice relaxation associated with a change in defect charge state at low temperature. The metastable behavior merely arises in this case from the existence of two defect configurations corresponding to slightly different total energies, which may be populated in either of two charge states. For such metastability to be detected the characteristic transformation temperatures should also not be too elevated, i.e., the elastic energy barrier separating the two configurations should not be too high. The corresponding defect complexes should therefore involve a highly mobile species.

Starting from these requirements, one may then extend the simple CC model of the $Fe_{(i)}Al_{(s)}$ ion pair in silicon to uncover a new class of metastable defects in semiconductors. Figure 11 shows a series of double-site CC diagrams that may be encountered for non-purely-ionic defect complexes. Again, we emphasize the basic difference between these models and previously proposed, large lattice-relaxation models. Case (a) in the figure is basically similar to the $Fe_{(i)}Al_{(s)}$ case, except that we no longer expect the definite relationship between E_1, E_2, and ΔE_b (see Fig. 1), which was a direct consequence of the Coulombic nature of the interaction potential. In such a case, however, all features of the metastable-defect behavior would be qualitatively similar to those described in Sec. II B. Case (b) is derived from (a) by simply inverting the relative magnitudes of the defect ionization energies (E_1,E_2) and reorientation energy (E_m in Fig. 1). For such a defect, the metastable configuration (Q_2) would be hardly detectable using DLTS, because most centers prepared in this configuration would have converted to the stable one (Q_1) before charge transfer at $Q=Q_2$ may be detected. Such difficulty would be expected in the search for the ⟨100⟩ configurations of some deep transition-metal—acceptor pairs

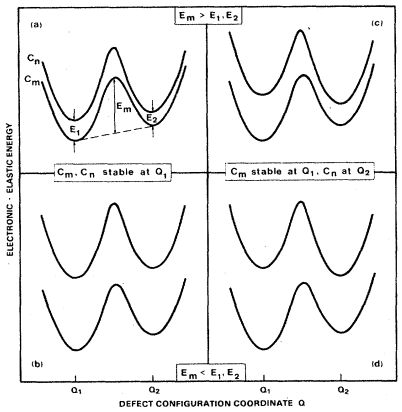

FIG. 11. Double-site CC diagrams for metastable-defect complexes in semiconductors. In cases (a) and (b) the stable configuration is the same for the two defect charge states C_m and C_n ($m = n \pm 1$). In cases (c) and (d) each configuration is stable in one charge state. The difference between (a) and (b), and (c) and (d), is in the relative magnitudes of E_1, E_2, and E_m, as defined in (a).

in silicon (see Sec. III B). It should be pointed out that this would no longer be the case, when probing the optical—rather than thermal—defect properties. Deep-level optical-spectroscopy (DLOS) measurements,[36] coupled to defect-charge-state control during sample cool-down, might help discover new examples of such metastable defects. The CC diagrams shown as panels (c) and (d) in Fig. 11 would correspond to defect complexes for which the stable configuration is not the same in the two charge states. Case (c) would be easily identifiable using the procedure described in this paper: Contrary to what is observed for $Fe_{(i)}Al_{(s)}$ (Fig. 3) [and would be observed for a defect such as (a)], the dominant DLTS feature in this case would not be the same for the two defect-state spectra characteristic of the system. This is what has been reported for the metastable M center in InP (Refs. 11 and 20) (see Sec. III D). Again, for a defect like (d) with higher ionization energies, optical measurements would greatly help understanding the metastable behavior. The recently discovered metastable properties of the vacancy-oxygen complex in silicon may be explained using such a CC diagram (see Sec. III C).

B. Transition-metal—acceptor pairs in silicon

As mentioned in the Introduction, the simple model of two electrostatically bound point charges satisfactorily describes most transition-metal—acceptor pairs in silicon.[5] All of these would therefore be expected to be observable in a ⟨100⟩ configuration, and give rise to a metastable-defect phenomenon of the type described in this paper. We have summarized in Table I the energy-level positions in the band gap expected for a series of ⟨100⟩-oriented pairs, starting from data recently compiled by Feichtinger *et al.*[37] for nearest-neighbor ⟨111⟩ configurations.[38] A search for these additional levels in Schottky diodes or

TABLE I. Energy-level positions of nearest-neighbor ⟨111⟩ (after Ref. 37) and next-nearest-neighbor ⟨100⟩ (calculated) transition-metal—shallow-acceptor pairs in silicon. Trap-level energies, in eV, are measured with respect to the conduction-band [$E(\ )$] or valence-band [$H(\ )$] edges.

Pair	⟨111⟩ configuration	⟨100⟩ configuration
$Fe_{(i)}B_{(s)}$	$H(0.10)$	$H(0.03)$
$Fe_{(i)}Al_{(s)}$	$H(0.20)$	$H(0.13)$
$Fe_{(i)}Ga_{(s)}$	$H(0.24)$	$H(0.17)$
$Mn_{(i)}B_{(s)}$	$E(0.55)$	$E(0.62)$
$Mn_{(i)}Al_{(s)}$	$E(0.45)$	$E(0.52)$
$Mn_{(i)}Ga_{(s)}$	$E(0.41, 0.43)$	$E(0.48, 0.50)$
$Cr_{(i)}B_{(s)}$	$H(0.29)$	$H(0.22)$
$Cr_{(i)}Al_{(s)}$	$H(0.45, 0.52)$	$H(0.38, 0.45)$
$Cr_{(i)}Ga_{(s)}$	$H(0.47, 0.48)$	$H(0.40, 0.41)$

p-n junctions, following reverse-bias [see Fig. 3(a)] cool-down, should provide a critical evaluation of the simple ionic model for these pairs. $Mn_{(i)}$-acceptor, $Cr_{(i)}Al_{(s)}$, and $Cr_{(i)}Ga_{(s)}$ pairs, which have levels deep in the band gap, would be expected to correspond to case (b) in Fig. 11. Detection of the ⟨100⟩ configuration of these pairs is therefore likely to be difficult, as discussed above. The ⟨100⟩-oriented $Fe_{(i)}B_{(s)}$ pair is also expected to escape DLTS detection, since the corresponding energy level is so shallow. Indirect experimental evidence for this configuration has been given, however, using short-range electronic dissociation of ⟨111⟩ pairs at low temperature.[7]

The $Fe_{(i)}In_{(s)}$ case has not been included in Table I, although a DLTS level, $H(0.16$ eV), has been reported for this pair.[39] Clearly, for such a center, which shows ⟨100⟩ symmetry as revealed by EPR,[5] the simple ionic model cannot be valid. One should not conclude, however, that the $H(0.16)$ level [hereafter, trap-level energies, in eV, are measured with respect to the conduction-band, $E(\ )$, or valence-band, $H(\ )$, edges] arises from the ⟨100⟩ pair configuration. The $Fe_{(i)}In_{(s)}$ pair may well correspond to a case such as (c) in Fig. 11, for which EPR and DLTS would not probe the same defect configuration! Deeper understanding of this interestingly different transition-metal—acceptor pair awaits future experimental investigations.

To end up with transition-metal—acceptor pairs, we should finally mention that $Co_{(i)}$-acceptor pairs with different configurations have been recently observed using Mössbauer spectroscopy;[40] all of these have eluded DLTS detection so far, however.[41]

C. Vacancy-oxygen center (A center) in silicon

The vacancy-oxygen (V-O) complex in silicon, commonly called the "A center," is one of the dominant radiation-induced defects in pulled material. It consists of a substitutional-oxygen impurity, off center in a ⟨100⟩ direction,[29] and introduces an acceptor level, $E(0.17)$, in the band gap.[42] It has been recently discovered that this electron trap is involved in a metastable reaction, which, we believe, may be explained in the light of the $Fe_{(i)}Al_{(s)}$

case. The original observation,[34] based on isothermal capacitance transients measurements, may be summarized as follows. When monitoring the capacitance relaxation associated with $E(0.17)$, part of the signal is found to transform into a faster component—corresponding to a shallower electron trap $E(0.10)$—under special pulsing conditions applied to the junction. For this to be observed,[34] the time between majority-carrier pulses, t_r, and the pulse width, t_p, should obey the relations

$$t_r \gg \tau_r = 7.5\times 10^{-13}\ \exp[(0.174\ \text{eV})/kT]\ \text{s} \quad (7)$$

and

$$t_p \ll \tau_p = 7.3\times 10^{-13}\exp[(0.145\ \text{eV})/kT]\ \text{s}\ . \quad (8)$$

Not all of the $E(0.17)$ signal can be transformed into $E(0.10)$, however. This led to the suggestion that two different defects were responsible for the $E(0.17)$ response: the V-O center for the unconvertible part of the signal, and another center (possibly being an impurity trapped by an A center), giving rise to the $E(0.17)\leftrightarrow E(0.10)$ transmutation behavior. The example of the $Fe_{(i)}Al_{(s)}$ pair reported in this paper makes it clear that such behavior may well arise from a single defect, i.e., the V-O center, provided that this defect may exist in an alternate, excited configuration. The arguments to be given below fully support this new interpretation.

The metastable-defect phenomenon involving $E(0.17)$ is also observable using the experimental procedure used for $Fe_{(i)}Al_{(s)}$ in Sec. II B, as illustrated in Fig. 12 and already pointed out by Benton and Levinson.[11] Whereas $E(0.17)$ is the unique electron trap detected at low temperature following zero-bias cooling of the sample [Fig. 12(b)], reverse-bias cooldown results in the subsequent additional observation of the shallow $E(0.10)$ level [Fig. 12(a)]. Consistently with Eqs. (7) and (8), the amplitude of this level is maximum for short pulse widths (t_p) and low rate-window settings e_0 (large t_r). It should be noted also that no complementary behavior of the $E(0.17)$ signal is observed in this case, as already pointed out in Ref. 11.

These observations look so much like the metastable behavior displayed by $Fe_{(i)}Al_{(s)}$ (cf. Figs. 12 and 3) that they call for a similar interpretation. A double-site CC diagram like Fig. 11(d) seems to be more appropriate in this case. A CC model of the center, consistent with the above experimental results, is shown in Fig. 13. This model assumes the existence of an excited configuration of the center, $(V\text{-O})^*$. The $E(0.17)$ and $E(0.10)$ levels are ascribed to transitions $(V\text{-O})^-$-$(V\text{-O})^0$ and $(V\text{-O})^{*-}$-$(V\text{-O})^{*0}$, respectively. The reason that we take $(V\text{-O})^*$, and not $(V\text{-O})$, as the stable configuration of the neutral center, will become clear later.

The above-mentioned experimental observations may now be simply explained. When cooling the sample with the bias off, the center is left in the $(V\text{-O})^-$ state (Fig. 13), and the $E(0.17)$ level is detected during subsequent DLTS measurements [Fig. 12(b)]. Cooling under applied reverse bias results in $(V\text{-O})^{*0}$ centers at low temperature (Fig. 13). Upon electron capture at the beginning of the DLTS run, part of $(V\text{-O})^{*-}$ transforms into $(V\text{-O})^-$ (rate τ_p^{-1}) before electron reemission, because of the low associated barrier height, and hence the reduced $E(0.10)$ signal height [Fig. 12(a)]. The transformation $(V\text{-O})^{*-}\rightarrow(V\text{-O})^-$ proceeds slowly during refilling periods (t_p) until completion, restoring the $E(0.17)$ DLTS signal. The isothermal capacitance transient observations of Jellison[34] may be understood as well. Clearly, for the $E(0.10)$-associated component to be observed, the time between pulses should be long enough to provide a large $(V\text{-O})^{*0}$ concentration, and the pulse width short enough to limit the $(V\text{-O})^{*-}\rightarrow(V\text{-O})^-$ configurational transformation. In this respect, the significance of Eq. (7) is simply that the barrier to $(V\text{-O})^0\rightarrow(V\text{-O})^{*0}$ transformation is lower than the activation energy for electron emission from $(V\text{-O})^-$.

The double-site CC model of the A center shown in Fig. 13 also sheds new light on the results of previous EPR studies in low-temperature-irradiated, n-type silicon.[43] In those EPR studies it was found that, in addition to the isolated vacancy, a defect identified as an excited configuration of the V-O pair, $(V\text{-O})^*_{100}$, was present immediately following irradiation at 20.4 K. Upon warming to $\sim$45 K, this defect was found to convert into the "normal" V-O configuration, with kinetics

$$\tau^{-1} = 4\times 10^{12}\exp[-(0.14\ \text{eV})/kT]\ \text{s}^{-1}\ . \quad (9)$$

The CC diagram proposed for the center offers a simple explanation for these results. During electron irradiation at low temperature, neutral V-O pairs are created in the

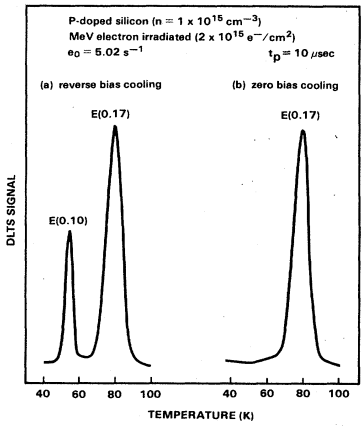

FIG. 12. DLTS spectra of V-O in silicon showing the result of cooling with (a) applied reverse bias, and (b) zero bias.

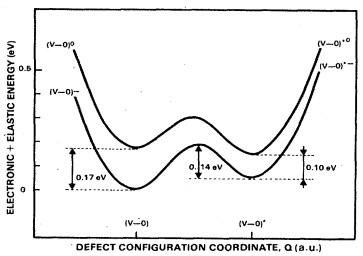

FIG. 13. Configuration-coordinate diagram for the V-O center in silicon. The excited $(V\text{-O})^*$ configuration explains the recently discovered metastable behavior of the defect.

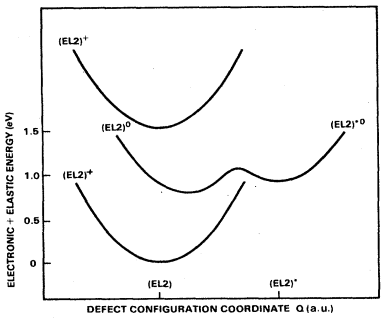

FIG. 14. Configuration-coordinate diagram for the EL2 center in GaAs. The metastable $(EL2)^{*0}$ configuration of the defect is responsible for the so-called photocapacitance quenching effect.

stable $(V\text{-}O)^{*0}$ configuration. Electron capture at the end of the irradiation produces the paramagnetic metastable $(V\text{-}O)^{*-}$ species, which transforms into $(V\text{-}O)^{-}$ upon annealing. We note that the kinetics of this transformation is indeed in good agreement with Eq. (8).

Although the CC diagram in Fig. 13 appears to account for most electrical and EPR data concerning the V-O center, more work is required to understand the microscopic structure of the excited $(V\text{-}O)^{*}$ configuration and the details of the configurational transformation.

D. EL2 center in GaAs and *M* center in InP

The EL2 center in GaAs and the M center in InP are two defects showing complex metastable behavior for which no definite microscopic explanation is available as yet. In this section we briefly discuss the applicability of double-site CC diagrams to describe these centers.

The EL2 center is responsible for the dominant deep level in melt-grown GaAs.[44] It is very unusual because of its anomalous optical properties at low temperature, most notably revealed by the persistent photocapacitance quenching effect.[33] These properties have been phenomenologically explained by the existence of a metastable configuration of the center, $(EL2)^{*}$, as illustrated on the CC diagram shown in Fig. 14. The EL2 center should not be considered, however, to be an additional example for the class of metastable defects presented in Fig. 11. In this case, indeed, the alternate $(EL2)^{*}$ configuration cannot be populated in either of the two defect charge states: only neutral centers may be prepared in this configuration. This is experimentally demonstrated by the optical inactivity of the $(EL2)^{*0}$ state, which, in fact, is responsible for the photocapacitance quenching effect. We therefore keep the widespread picture of this unusual phenomenon as being a consequence of very large lattice relaxation.

The M center in InP is the most recently discovered example of a metastable defect in covalent semiconductors.[11,12,20] For this electron-irradiation-induced defect, as for $Fe_{(i)}Al_{(s)}$ in silicon (Fig. 3), two different capacitance transient spectra are obtained, depending upon the bias condition applied to the sample during the cooldown to the initial measurement temperature. In this case, however, different DLTS signals are found to dominate the two characteristic defect-state spectra, contrary to what was observed for $Fe_{(i)}Al_{(s)}$. As already pointed out, such features may be qualitatively accounted for by a CC diagram such as Fig. 11(c). The CC model proposed by Stavola *et al.*[12] for this center is basically different and much more elaborate, involving extrinsic self-trapping and negative U simultaneously. The experimental observations are also more complicated than shortly summarized above, especially because of the apparent multielectron trapping nature of the M center. A complete discussion of all the results is beyond the scope of this paper. The present suggestion should therefore merely be considered as a hint for future studies concerning this defect.

IV. CONCLUSION

Defects that display complicated, metastable behavior are becoming more than exceptions among covalent semiconductor defects. A growing number of such centers have been discovered in the last years in silicon and compound semiconductors. The defect metastability reported in this paper is a new example of such phenomena. It has the unique feature, however, to take place at a well-identified point defect in silicon, the interstitial-iron—substitutional-aluminum pair. We are thus able to provide a detailed microscopic description of the phenomenon. This was generally not possible for previously investigated metastable reactions, involving structurally unidentified defects. The phenomenon is ascribed to charge-state-controlled, electrostatically driven reorientation of the pair between the $\langle 111 \rangle$ and $\langle 100 \rangle$ configurations. It is a direct consequence of the Coulombic nature of the interaction potential between iron and aluminum. Similar behavior is therefore expected for other ion pairs in semiconductor hosts, and particularly for other transition-metal—acceptor pairs in silicon.

The $Fe_{(i)}Al_{(s)}$ defect in silicon is also different from previously studied metastable centers in that it cannot be classified among very large lattice-relaxation centers. None of the characteristic features of such centers, including carrier capture by the multiphonon emission mechanism, and large Stokes shifts between optical and thermally activated transition energies, would indeed be expected for this defect. The double-site CC diagram proposed for $Fe_{(i)}Al_{(s)}$ therefore constitutes an alternative to large lattice-relaxation models for the understanding of metastable defect phenomena in semiconductors. We have shown how this concept may be extended to non-purely-ionic defect complexes. The vacancy-oxygen center in silicon appears to belong to this new class of metastable centers. The methods for identifying such defects being well defined, further examples should be discovered in the near future.

ACKNOWLEDGMENTS

The authors wish to thank Professor J. C. Pfister, Dr. C. A. J. Ammerlaan, and Dr. A. Bourret for fruitful dis-

cussions. Thanks are also due Dr. C. A. J. Ammerlaan and Dr. P. Wagner for providing the samples used in this work, Dr. G. Auvert for expert assistance in the laser-irradiation experiments, and Dr. J. J. Van Kooten for making a report of his work available prior to publication. Critical reading of the manuscript by Dr. G. Vincent is gratefully acknowledged.

---

[1]For a recent review on transition metals in silicon, see E. R. Weber, Appl. Phys. A **30**, 1 (1983).

[2]J. D. Gerson, L. J. Cheng, and J. W. Corbett, J. Appl. Phys. **48**, 4821 (1977).

[3]A. Chantre, J. Phys. (Paris) Colloq. **44**, C5-269 (1983).

[4]K. Wünstel and P. Wagner, Appl. Phys. A **27**, 207 (1982).

[5]G. W. Ludwig and H. H. Woodbury, in *Solid State Physics,* edited by H. Ehrenreich, Frederick Seitz, and David Turnbull (Academic, New York, 1962), Vol. 13, p. 223.

[6]K. Graff and H. Pieper, J. Electrochem. Soc. **128**, 669 (1981).

[7]L. C. Kimerling and J. L. Benton, in Defects in Semiconductors 1982 [Physica (Utrecht) **116B**, 297 (1983)].

[8]H. Conzelmann, K. Graff, and E. R. Weber, Appl. Phys. A **30**, 169 (1983).

[9]H. Reiss, C. S. Fuller, and F. J. Morin, Bell Syst. Tech. J **35**, 535 (1956).

[10]L. C. Kimerling, J. L. Benton, and J. J. Rubin, in *Defects and Radiation Effects in Semiconductors 1980, 11th International Conference on Defects and Radiation Effects in Semiconductors, Nice, 1978,* edited by J. H. Albany (IOP, London, 1979), p. 217.

[11]J. L. Benton and M. Levinson, in *Defects in Semiconductors II,* edited by S. Mahajan and J. W. Corbett (North-Holland, New York, 1983), p. 95.

[12]M. Stavola, M. Levinson, J. L. Benton, and L. C. Kimerling, Phys. Rev. B **39**, 832 (1984).

[13]A. Chantre and D. Bois (unpublished).

[14]A. Chantre, M. Kechouane, and D. Bois, in *Defects in Semiconductors II,* Ref. 11, p. 547.

[15]N. H. Sheng and J. L. Merz, J. Appl. Phys. **55**, 3083 (1984).

[16]A. Chantre, M. Kechouane, and D. Bois, in Defects in Semiconductors 1982 [Physica (Utrecht) **116B**, 547 (1983)].

[17]A. Chantre, M. Kechouane, G. Auvert, and D. Bois, Appl. Phys. Lett. **43**, 98 (1983).

[18]These energies are deduced from thermal-emission-rate data obtained for the levels, after correction for the temperature dependence of thermal velocity ($\propto T^{0.5}$) and effective density of states ($\propto T^{1.5}$).

[19]A. Chantre, Appl. Phys. Lett. **46**, 263 (1985).

[20]M. Levinson, J. L. Benton, and L. C. Kimerling, Phys. Rev. B **27**, 6216 (1983).

[21]In these measurements, the bias was turned back on at the end of the anneal time for the fast cooldown to 77 K. A slight H1$\rightarrow$H2 transformation may have taken place at the beginning of the cooldown period, since the onset of the $b\rightarrow a$ transition is so close to 195 K (see Fig. 5).

[22]J. Frenkel, Phys. Rev. **54**, 647 (1938).

[23]L. C. Kimerling and J. L. Benton, Appl. Phys. Lett. **39**, 410 (1981).

[24]The small shift in peak position ($\sim$3 K) detected for H2 must be ascribed to another electric-field-enhanced emission mechanism. Models of field-enhanced emission processes have been reported for non-Coulombic centers; see, for example, G. Vincent, A. Chantre, and D. Bois, J. Appl. Phys. **50**, 5484 (1979).

[25]G. L. Miller, D. V. Lang, and L. C. Kimerling, Ann. Rev. Mater Sci. **7**, 377 (1977).

[26]For $p=1\times10^{16}$ cm^{-3}, the Fermi level crosses the H2 level downward at $T\sim230$ K, i.e., above the two $a\rightarrow b$ and $b\rightarrow a$ transformation temperatures (see Fig. 5).

[27]For iron in the $Fe_{(i)}^{+}$ charge state, the elastic energy barrier separating the two T_d sites is almost symmetrical (see Fig. 10). Transformation $b\rightarrow a$ is therefore merely controlled by the average barrier height.

[28]J. J. Van Kooten, G. A. Weller, and C. A. J. Ammerlaan, Phys. Rev. B **30**, 4564 (1984).

[29]G. D. Watkins and J. W. Corbett, Phys. Rev. **121**, 1001 (1961).

[30]M. Stavola, J. R. Patel, L. C. Kimerling, and P. E. Freeland, Appl. Phys. Lett. **42**, 73 (1983).

[31]M. Stavola and L. C. Kimerling, J. Appl. Phys. **54**, 3897 (1983).

[32]D. V. Lang and R. A. Logan, Phys. Rev. B **19**, 1015 (1979).

[33]G. Vincent, D. Bois, and A. Chantre, J. Appl. Phys. **53**, 3643 (1982).

[34]G. E. Jellison, J. Appl. Phys. **53**, 5715 (1982).

[35]C. H. Henry and D. V. Lang, Phys. Rev. B **15**, 989 (1977).

[36]A. Chantre, G. Vincent, and D. Bois, Phys. Rev. B **23**, 5335 (1981).

[37]H. Feichtinger, J. Oswald, R. Czaputa, P. Vogl, and K. Wünstel, in Proceedings of the 13th International Conference on Defects in Semiconductors, 1984 [J. Electron. Mater. (to be published)].

[38]Energy levels for hole traps have been calculated using Eq. (3). For electron traps, it is straightforward to note that this expression becomes $E_2=E_1+\Delta E_b=E_1+0.071$ eV.

[39]R. Sauer and J. Weber, in Defects in Semiconductors 1982 [Physica (Utrecht) **116B**, 195 (1983)].

[40]W. Bergholz, in Defects in Semiconductors 1982 [Physica (Utrecht) **116B**, 312 (1983)].

[41]E. Scheibe and W. Schröter, in Defects in Semiconductors 1982 [Physica (Utrecht) **116B**, 318 (1983)]

[42]L. C. Kimerling, in *Radiation Effects in Semiconductors, Dubrovnik, 1976,* edited by N. B. Urli and J. W. Corbett (IOP, Bristol, 1977).

[43]G. D. Watkins, in *Lattice Defects and Radiation Effects in Semiconductors, Freiberg, Germany, 1974,* edited by F. A. Huntley (IOP, Bristol, 1975), p. 1.

[44]For a recent review on this center, see G. M. Martin and S. Makram-Ebeid, in *Deep Centers in Semiconductors,* edited by S. T. Pantelides (Gordon and Breach, London, in press).